Video Article

A Silicon-tipped Fiber-optic Sensing Platform with High Resolution and Fast Response

Guigen Liu*[1], Qiwen Sheng*[1], Weilin Hou[2], Matthew L. Reinke[3], Ming Han[1,4]

[1]Department of Electrical and Computer Engineering, Michigan State University

[2]Naval Research Laboratory, Stennis Space Center

[3]Oak Ridge National Laboratory

[4]Department of Electrical and Computer Engineering, University of Nebraska-Lincoln

*These authors contributed equally

Correspondence to: Ming Han at mhan@egr.msu.edu

URL: https://www.jove.com/video/59026
DOI: doi:10.3791/59026

Keywords: Fiber-optic sensing, Fabry-Perot interferometer, Silicon, temperature measurement, flow sensors, bolometry

Date Published: 12/18/2018

Citation: Liu, G., Sheng, Q., Hou, W., Reinke, M.L., Han, M. A Silicon-tipped Fiber-optic Sensing Platform with High Resolution and Fast Response. *J. Vis. Exp.* (), e59026, doi:10.3791/59026 (2018).

Abstract

In this article, we introduce an innovative and practically promising fiber-optic sensing platform (FOSP) that we proposed and demonstrated recently. This FOSP relies on a silicon Fabry-Perot interferometer (FPI) attached to the fiber end, referred to as Si-FOSP in this work. The Si-FOSP generates an interferogram determined by the optical path length (OPL) of the silicon cavity. Measurand alters the OPL and thus shifts the interferogram. Due to the unique optical and thermal properties of the silicon material, this Si-FOSP exhibits an advantageous performance in terms of sensitivity and speed. Furthermore, the mature silicon fabrication industry endows the Si-FOSP with excellent reproducibility and low cost toward practical applications. Depending on the specific applications, either a low-finesse or high-finesse version will be utilized, and two different data demodulation methods will be adopted accordingly. Detailed protocols for fabricating both versions of the Si-FOSP will be provided. Three representative applications and their according results will be shown. The first one is a prototype underwater thermometer for profiling the ocean thermoclines, the second one is a flow meter to measure flow speed in the ocean, and the last one is a bolometer used for monitoring exhaust radiation from magnetically confined high-temperature plasma.

Video Link

The video component of this article can be found at https://www.jove.com/video/59026/

Introduction

Fiber-optic sensors (FOSs) have been the focus for many researchers due to its unique properties, such as its small size, its low cost, its light weight, and its immunity to electromagnetic interference (EMI)[1]. These FOSs have found wide applications in many areas such as environmental monitoring, ocean surveillance, oil exploration, and industrial process among others. When it comes to the temperature-related sensing, the traditional FOSs are not superior in terms of resolution and speed for the cases where measurement of minute and fast temperature variations is desirable. These limitations stem from the optical and thermal properties of the fused silica material on which many traditional FOSs are based. On one hand, the thermo-optic coefficient (TOC) and thermal expansion coefficient (TEC) of silica are 1.28×10^{-5} RIU/°C and 5.5×10^{-7} m/(m·°C), respectively; these values lead to a temperature sensitivity of only about 13 pm/°C around the wavelength of 1550 nm. On the other hand, the thermal diffusivity, which is a measure of the speed of temperature change in response to thermal energy exchange, is only 1.4×10^{-6} m^2/s for silica; this value is not superior for improving the speed of silica-based FOSs.

The fiber-optic sensing platform (FOSP) reported in this article breaks the above limitations of fused silica-based FOSs. The new FOSP utilizes crystalline silicon as the key sensing material, which forms a high-quality Fabry-Perot interferometer (FPI) on the end of the fiber, here referred to as silicon-tipped FOSP (Si-FOSP). **Figure 1** shows the schematic and operational principle of the sensor head, which is the core of the Si-FOSP. The sensor head essentially consists of a silicon FPI, whose reflection spectrum features a series of periodic fringes. Destructive interference occurs when the OPL satisfies $2nL=N\lambda$, where n and L are the refractive index and length of the silicon FP cavity, respectively, and N is an integer that is the order of the fringe notch. Therefore, positions of the interference fringes are responsive to the OPL of the silicon cavity. Depending on the specific applications, the silicon FPI can be made into two types: low-finesse FPI and high-finesse FPI. The low-finesse FPI has a low reflectivity for both ends of the silicon cavity, while the high-finesse FPI has a high reflectivity for both ends of the silicon cavity. The reflectivities of silicon-air and silicon-fiber interfaces are roughly 30% and 18%, thus the sole silicon FPI shown in **Figure 1a** is essentially a low-finesse FPI. By coating a thin high-reflectivity (HR) layer on both ends, a high-finesse silicon FPI is formed (**Figure 1b**). Reflectivity of the HR coating (either dielectric or gold) can be as high as 98%. For both types of Si-FOSP, both n and L increase when temperature increases. Thus, by monitoring the fringe shift, the temperature variation can be deduced. Note that for the same amount of wavelength shift, the high-finesse FPI gives a better discrimination due to the much narrower fringe notch (**Figure 1c**). While the high-finesse Si-FOSP has better resolution, the low-finesse Si-FOSP has a larger dynamic range. Therefore, the choice between these two versions depends on the requirements of a specific

Copyright © 2018 Journal of Visualized Experiments

application. Furthermore, due to the large difference in full width at half maximum (FWHM) of the low-finesse and high-finesse silicon FPIs, their signal demodulation methods are different. For example, the theoretical FWHM of 1.5 nm is reduced by about 50 times to only 30 pm when both ends of the sole silicon FPI are coated with a 98% HR layer. Therefore, for the low-finesse Si-FOSP, a high-speed spectrometer would suffice for the data collection and processing, while a scanning laser should be used to demodulate the high-finesse Si-FOSP due to the much narrower FWHM that cannot be resolved well by the spectrometer. The two demodulation methods will be explained in the protocol.

The silicon material chosen here is superior for temperature sensing in terms of resolution. As a comparison, the TOC and TEC of silicon are $1.5x10^{-4}$ RIU/°C and $2.55x10^{-6}$ m/(m·°C), respectively, leading to a temperature sensitivity of around 84.6 pm/°C which is about 6.5 times higher than that of all silica-based FOSs[2]. In addition to this much higher sensitivity, we have demonstrated an average wavelength tracking method to reduce the noise level and thus improve the resolution for a low-finesse sensor, leading to a temperature resolution of $6x10^{-4}$ °C [2], in comparison to the resolution of 0.2 °C for an all silica-based FOS[3]. The resolution is further improved to be $1.2x10^{-4}$ °C for a high-finesse version[4]. The silicon material is also superior for sensing in terms of speed. As a comparison, the thermal diffusivity of silicon is $8.8x10^{-5}$ m^2/s, which is more than 60 times higher than that of silica[2]. Combined with a small footprint (*e.g.*, 80 µm diameter, 200 µm thickness), the response time of 0.51 ms for a silicon FOS has been demonstrated[2], in comparison to the 16 ms of a micro-silica-fiber coupler tip temperature sensor[5]. Although some research work related to temperature measurement using very thin silicon film as the sensing material has been reported by other groups[6,7,8,9], none of them possesses the performance of our sensors in terms of either resolution or speed. For example, the sensor with a resolution of only 0.12 °C and a long response time of 1 s was reported.[7] A better temperature resolution of 0.064 °C has been reported[10]; however, the speed is limited by the relatively bulky sensor head. What makes the Si-FOSP unique lies in the new fabrication method and data processing algorithm.

Besides the above advantages for temperature sensing, the Si-FOSP can also be developed into a variety of temperature-related sensors aiming at measuring different parameters, such as gas pressure[11], air or water flow[12,13,14], and radiation[4,15]. This article presents a detailed description of the sensor fabrication and signal demodulation protocols along with three representative applications and their results.

Protocol

1. Fabrication of Low-Finesse Sensors

1. Fabricate the silicon pillars. Pattern a piece of 200-µm-thick double-side-polished (DSP) silicon wafer into standalone silicon pillars (**Figure 2a**), using standard micro-electro-mechanical system (MEMS) fabrication facilitates.
   NOTE: The patterned wafer is bonded on another larger silicon wafer using a thin layer of photoresist. The bonding force of the photoresist is strong enough to hold the pillars upright, but also weak enough to detach from the substrate for later steps.
2. Prepare the lead-in fiber. Strip off the plastic coating of the distal end of a single-mode optical fiber. Clean the stripped section using a lens tissue dipped with alcohol. Cleave the cleaned fiber using an optical fiber cleaver.
3. Apply a thin layer of UV-curable glue on the end-face of the cleaved lead-in fiber (**Figure 2b**). Put a little drop of UV-curable glue on a piece of glass slide. Thin the glue layer by spin-coating or manually swinging the glass slide. Transfer the glue layer to the fiber end by pressing the end face of the lead-in fiber against the glass slide.
4. Attach a silicon pillar to the fiber end. Align the lead-in fiber with one of the silicon pillars, meanwhile monitor the real-time reflection spectrum of the silicon FPI using a spectrometer. Use a UV lamp to cure the glue when a satisfactory spectrum is observed (**Figure 2c**).
   NOTE: In general, the curing process takes around 10 to 15 minutes.
5. Detach the sensor from the substrate. After the UV glue is fully cured, lift up the lead-in fiber along with the silicon pillar detached from the substrate (**Figure 2d**).
   NOTE: Some residual photoresist is remained on the top surface of the silicon pillar (**Figure 2e**). For most cases, the photoresist residual does not affect the function of the sensor. If needed, the photoresist layer can be removed by alcohol.
6. Examine the fabricated sensor head. Use a microscope to examine the geometry of the fabricated sensor head. A typical image of a sensor successfully fabricated is seen in **Figure 2f**.

2. Fabrication of High-Finesse Sensors

1. Coat both sides of a silicon wafer with high-reflectivity mirrors. Coat one side of a 75-µm-thick double-side-polished silicon wafer with a 150 nm thick gold layer using a sputtering coating machine, and coat the other side with a high-reflectivity (HR) dielectric mirror.
   NOTE: The dielectric HR coating was done by an outside company; reflectivity of this coating was tested to be no less than 98% by the company. However, detailed materials and structure of the coating are unknown due to the proprietary protection by the company, see the **Table of Materials** for more information.
2. Prepare the collimated lead-in fiber. Splice a short section of graded-index multi-mode fiber (GI-MMF) with a single-mode fiber, and then, under an optical microscope, cleave the GI-MMF with a quarter of the period of the light trajectory within the MMF left to form a fiber collimator (**Figure 3a**).
   NOTE: The GI-MMF is used to expand the modal field diameter so that a spectrum with a better visibility can be obtained[4,16]. The length of the GI-MMF, which is around 250 µm in this work, is exactly one quarter of the period of the ray trajectory.
3. Attach a fragmented double-side coated silicon to the lead-in fiber. Assemble a high-finesse sensor by following the similar steps of attaching a silicon pillar to the fiber end for fabricating low-finesse sensors (steps 1.3 – 1.5).
   NOTE: The side with the dielectric coating will be attached to the collimator to let in the coming light (**Figure 3b, 3 c**). In this case, the previous silicon pillar is replaced with a silicon fragment, which was not patterned. In the future, the patterned silicon wafer will be coated with the high-reflectivity mirrors, so that the sensors are more uniform and easier for fabrication. The difference in the fabrication steps of 1.3-1.5 is that a reflection spectra notch with proper visibility should be obtained first before the glue was transferred to the end face of the collimator.
4. Polish the irregularly-shaped silicon fragment into a circular shape using a fiber polishing machine.
5. Examine the fabricated sensor head. Use a microscope to examine the sensor head to make sure a desirable circular shape is achieved (**Figure 3d**).

3. Signal Demodulation for Low-Finesse Si-FOSP

NOTE: The system used for demodulating the low-finesse Si-FOSP is shown in **Figure 4a**. The following detailed steps help set up the system and perform the data processing.

1. Connect a C-band broadband source to port 1 of an optical circulator.
2. Splice port 2 of the optical circulator with the lead-in fiber of a low-finesse sensor.
3. Connect port 3 of the optical circulator to a high-speed spectrometer which communicates with a computer for data storage.
4. Check the spectrum of the sensor to make sure the system works properly. See the typical spectrum shown in **Figure 4b**.

4. Signal Demodulation for High-Finesse Si-FOSP

NOTE: The system used for demodulating the high-finesse Si-FOSP is shown in **Figure 5a**. The following detailed steps help set up the system and do the data post-processing.

1. Sweep a tunable DFB laser using a current controller.
   NOTE: The peak-to-peak sweeping voltage, which varies for different lasers and controllers, should be large enough to cover the spectrum notch.
2. Connect the output of the tunable laser to port 1 of an optical circulator.
3. Splice port 2 of the optical circulator to a high-finesse sensor.
4. Connect port 3 of the optical circulator to a photodetector.
5. Use a data acquisition device to read the output of the photodetector, which is stored by a computer.
6. Check the spectrum of the sensor to make sure the system works properly. See a typical frame of spectrum shown in **Figure 5b**. Find the valley position using a polynomial curve fitting.

Representative Results

Si-FOSP as an underwater thermometer for profiling ocean thermoclines

Recent oceanographic research has demonstrated that the blurring of underwater imaging stems not only from turbidity in contaminated waters but also from temperature microstructures in clean ocean[17,18]. The latter effect has been the focus of many oceanographers, aiming to find an effective way to rectify the blurred images[19], to better understand and improve optical communication in the water, as well as to develop means of quantifying turbulence in the ocean[20,21]. The Si-FOSP used as a temperature sensor has been demonstrated to outperform its current counterpart for measuring the swift temperature variations of water turbulence[22]. In this application, the low-finesse sensor shown in **Figure 1a** along with the signal demodulation system in **Figure 4a** is used. Given the superior performance of the Si-FOSP temperature sensor, it has been developed into a patented underwater instrument[23] (**Figure 6a**), which is intended to characterize the thermoclines of open waters. This sub-section presents the results of a field testing (**Figure 6b**) on the Flint Creek Reservoir in Mississippi, USA.

Figure 6c shows a measured thermocline of the Flint Creek Reservoir on September 13th, 2016. The blue curve was obtained by the Si-FOSP temperature sensor, while the red and black curves were obtained by two reference commercial CTDs (oceanography instruments for measuring conductivity, temperature, and depth of seawater). Obviously, the Si-FOSP temperature sensor agrees with the reference sensors, but with more details of the temperature structures (see the inset of **Figure 6c**) that may give a bunch of extra information. The more informative data collected by the Si-FOSP temperature sensor is expected to impact many branches of oceanographic research.

Si-FOSP as a large-dynamic-range flow sensor

Measurement of gas or liquid flows is pivotal to various academic and industrial sectors, which may provide important information to oceanography, weather research, process controls, transportation, and environment monitoring. Representative results of the Si-FOSP working as a flow sensor will be demonstrated. A low-finesse Si-FOSP is used for this application. However, since this flow sensor needs the sensing head to be actively heated by another laser, the system used is slightly different from that shown in **Figure 4a**. Specifically, an extra heating laser is used to activate the sensing head, and a detailed description of the system for flow measurement has been reported[12,13,14].

Figure 7a shows the Si-FOSP flow sensor situated in a water tank, with a side-by-side comparison to a commercial flow sensor. Obviously, readout of the fiber sensor generally agrees with that of the commercial flow sensor, as shown in **Figure 7b**; however, the Si-FOSP flow sensor exhibits a much clearer response when the water flows calm down, as illustrated by the close-up view in **Figure 7b**.

Si-FOSP as an EMI-immune bolometer for high-temperature plasma physics

Scientists investigating high-temperature plasma physics in tokamaks are trying to convert the exhaust power of magnetic confinement fusion reactors into photon emission to mitigate the heat flux impinged onto the plasma facing components[24]. **Figure 8a** shows the interior of a tokamak[25]. The photon emission is typically measured by a bolometer. While resistive and infrared video bolometers have achieved a noise equivalent power density (NEPD) of 0.2 W/m^2 and 0.23 W/m^2, respectively, in a laboratory environment[26,27], they are vulnerable to the harsh environment associated with the high-temperature plasma. The Si-FOSP reported in this work stands out as a promising alternative to the existing bolometers. To obtain a resolution as high as possible, the high-finesse version shown in **Figure 1b** will be used. Also, slightly different from the single-channel demodulation system shown in **Figure 5a**, a two-channel system will be used to compensate for the drift of the laser by using another dummy reference[4,15].

Figure 8b gives the measured results of one Si-FOSP bolometer in a laboratory environment, in comparison with another resistive bolometer. Our Si-FOSP bolometer has a NEPD of 0.27 W/m^2 which is close to those of the electronic counterparts[26,27]. Noting that the Si-FOSP bolometer has inherent resistance to the EMI typically found in high-temperature plasma physics, it is expected to hold great promises toward practical applications in tokamaks.

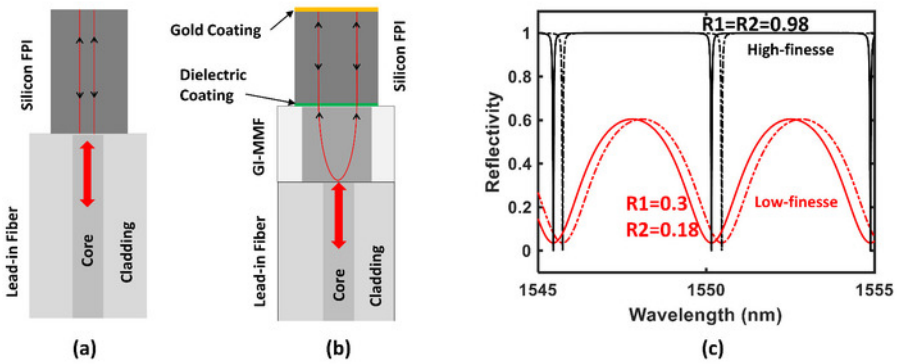

Figure 1: Schematics showing the low-finesse (a) and high-finesse (b) Si-FOSP. (c) Simulated reflection spectra of the two versions of Si-FOSPs with a 75 µm thick silicon cavity. The minute shift of the spectrum (from solid to dashed curves) is much better discriminated by the high-finesse sensor. Please click here to view a larger version of this figure.

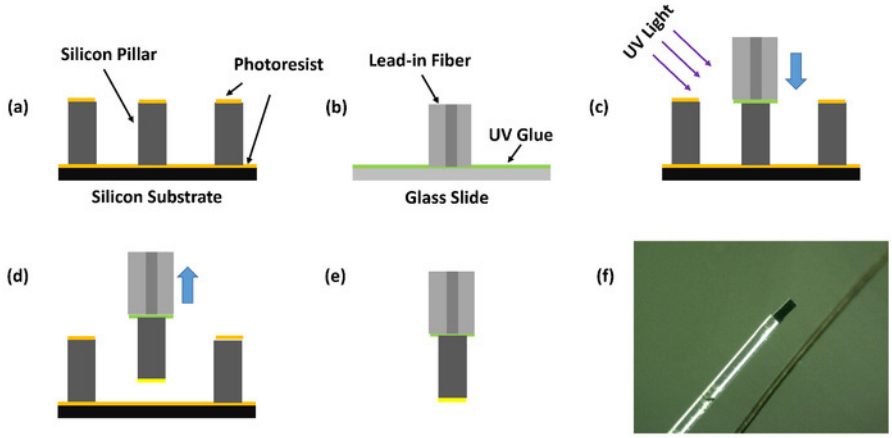

Figure 2: Fabrication of low-finesse Si-FOSPs. (a)-(e) Schematic fabrication steps and (f) image of a fabricated sensor head compared with a human hair. Please click here to view a larger version of this figure.

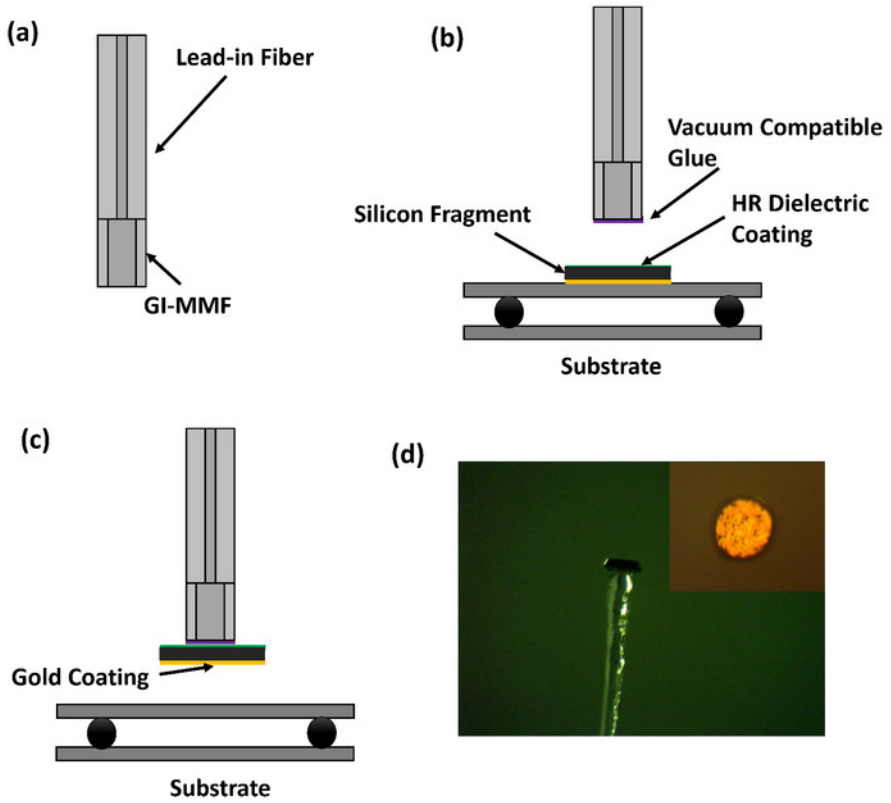

Figure 3: Fabrication of high-finesse Si-FOSPs. (a)-(c) Schematic fabrication steps and (d) image of one fabricated sensor. Inset in (d) shows the top view of the sensor head. GI-MMF, graded-index multi-mode fiber; HR, high-reflectivity. Please click here to view a larger version of this figure.

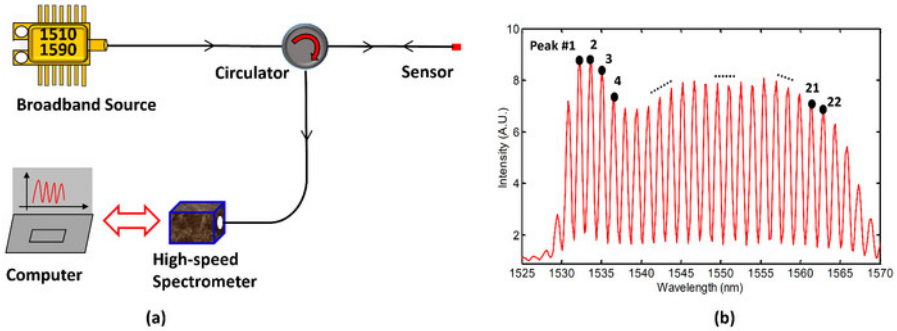

Figure 4: (a) Schematic system of the demodulation system and (b) one typical frame of reflection spectrum for a low-finesse Si-FOSP. Please click here to view a larger version of this figure.

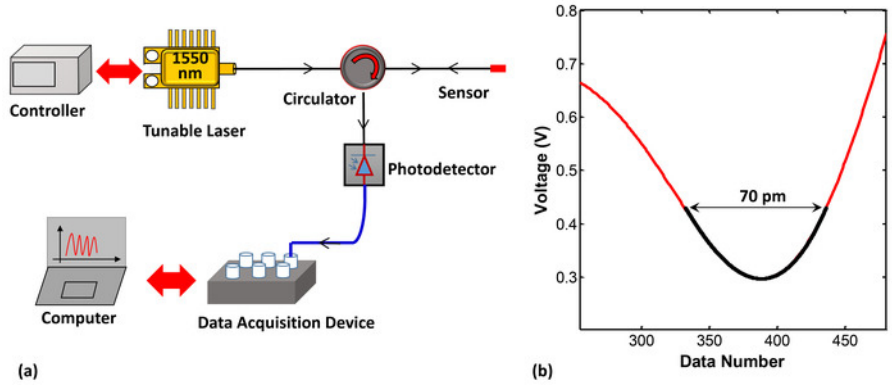

Figure 5: (a) Schematic system of the demodulation system and (b) one typical frame of scanned spectrum for a high-finesse Si-FOSP. Please click here to view a larger version of this figure.

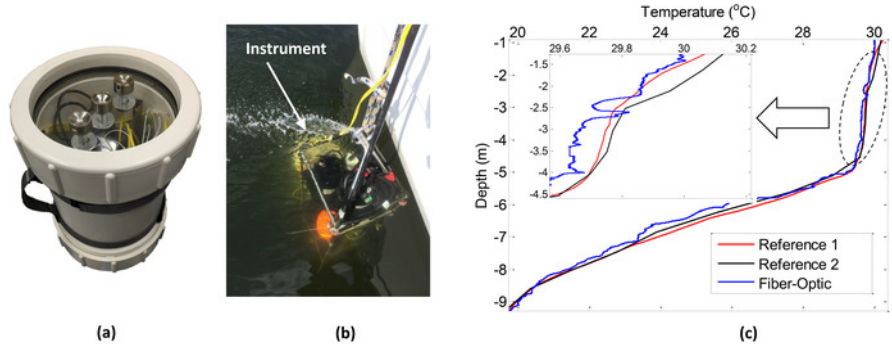

Figure 6: Representative results as an underwater thermometer. (a) Image and (b) field deployment of the prototyped sensor instrument. (c) Measured thermocline of Flint Creek Reservoir, Mississippi, USA, on September 13th, 2016. Please click here to view a larger version of this figure.

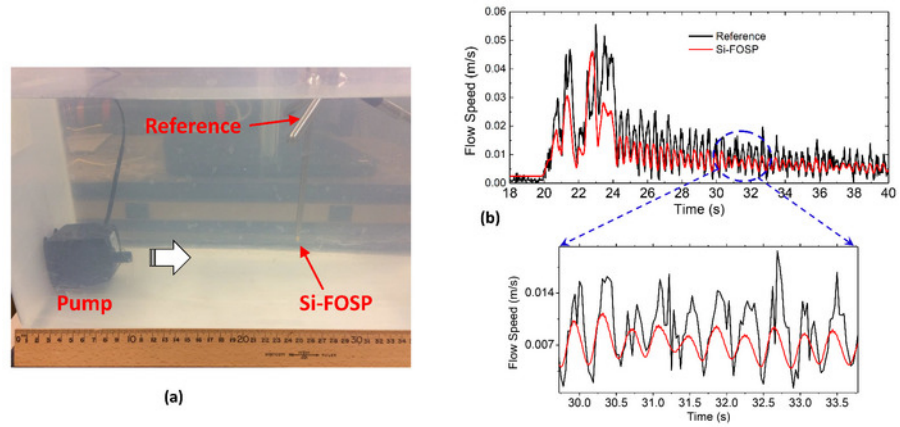

Figure 7: Representative results as a flow sensor. (a) Image of the flow testing arrangement and (b) comparison between the measured flow field by the Si-FOSP and that of a commercial flow sensor. Please click here to view a larger version of this figure.

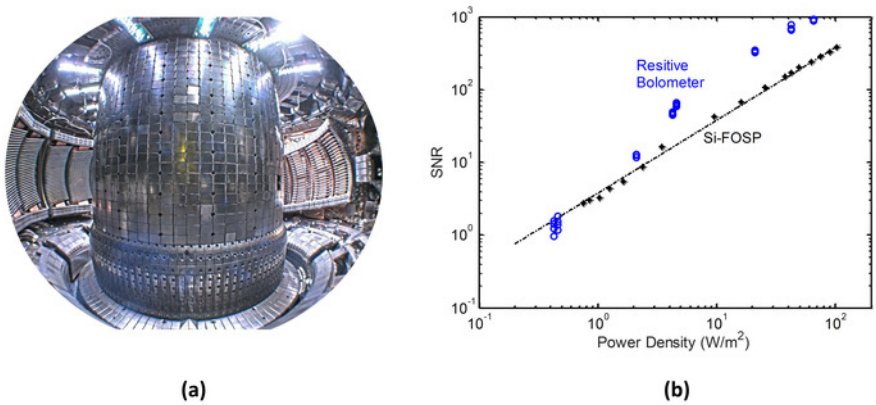

Figure 8: Representative results as a bolometer for high-temperature plasma research. (a) Image of the inner high-temperature plasmas space in a tokamak[25] and (b) measured results in a laboratory environment. This figure is adopted and modified from Wikimedia Commons. Please click here to view a larger version of this figure.

Discussion

The choice of the size (length and diameter) of the silicon FPI is made upon the tradeoff between requirements on the resolution and speed. In general, a smaller size provides a higher speed but also reduces the resolution[2]. A short length is advantageous for obtaining a higher speed, but it is not superior for obtaining a high resolution due to the expanded FWHM of the reflection notches. Using HR coatings to reduce the FWHM can help improve the resolution, but it will limit the dynamic range due to the signal demodulation using laser scanning. A smaller diameter increases the speed, but the diameter should be larger than the modal field diameter of the lead-in fiber so that a good spectrum can be achieved. It is, however, also found that a silicon diameter larger than that of the fiber helps improve the sensitivity for bolometry due to the reduced conduction heat loss to the fiber[4].Therefore, the choice of the sensor size is highly dependent on the specific applications.

Although we only demonstrate the very basic structures, fabrication protocols, and signal demodulation systems for the Si-FOSP, there are various techniques that can fit it into other applications or further improve the performance. For example, instead of using UV-curable glue to attach the sensor, a fusion splicing technique can be applied to elevate the operation temperature above 1,000 °C[28]. With such a high operation temperature, innovative types of photonic devices can be made, such as micro-heaters, infrared emitters, and bubble generators. Another example is the self-temperature compensated gas pressure sensing using the wavelength difference when the heating laser is turned on and off[11]. Furthermore, through the development of novel peak recognition techniques[29,30], temperature measurement over extended dynamic range can be realized.

Disclosures

An U.S. patent (No. 9995628 B1) has been issued to protect the related technologies.

Acknowledgements

This work was supported by U.S. Naval Research Laboratory (Nos. N0017315P0376, N0017315P3755); U.S. Office of Naval Research (Nos. N000141410139, N000141410456); U.S. Department of Energy (Nos. DE-SC0018273, DE-AC02-09CH11466, DE-AC05-00OR22725).

References

1. Lee, B. Review of the present status of optical fiber sensors. *Optical Fiber Technology.* **9**, 57-79 (2003).
2. Liu, G., Han, M., and Hou, W. High-resolution and fast-response fiber-optic temperature sensor using silicon Fabry-Perot cavity. *Optics Express.* **23**, 7237-7247 (2015).
3. Hatta, A. M., Rajan, G., Semenova, Y., and Farrell, G., SMS fibre structure for temperature measurement using a simple intensity-based interrogation system. *Electronics Letters.* **45**, 1069-2 (2009).
4. Sheng, Q., Liu, G., Reinke, M. L., and Han, M., A fiber-optic bolometer based on a high-finesse silicon Fabry-Perot interferometer. *Review of Scientific Instruments.* 065002 (2018).
5. Ding, M., Wang, P., and Brambilla, G., Fast-response high-temperature microfiber coupler tip thermometer. *IEEE Photonics Technology Letters.* **24**, 1209-1211 (2012).
6. Berthold, J. W., Reed, S. E., and Sarkis, R. G., Reflective fiber optic temperature sensor using silicon thin film. *Optical Engineering.* **30**, 524-528 (1991).
7. Kajanto, I., and Friberg, A. T., A silicon-based fibre-optic temperature sensor. *Journal of Physics E: Scientific Instruments.* **21**, 652-656 (1988).
8. Schultheis, L., Amstutz, H., and Kaufmann, M., Fiber-optic temperature sensing with ultrathin silicon etalons. *Optics Letters.* **13**, 782-784 (1988).
9. Zhang, S. *et al.* Temperature characteristics of silicon core optical fiber Fabry-Perot interferometer. *Optics Letters.* **40**, 1362-1365 (2015).

Copyright © 2018 Journal of Visualized Experiments

10. Cocorullo, G., Corte, F. G. D., Iodice, M., Rendina, I., and Sarro, P. M., A temperature all-silicon micro-sensor based on the thermo-optic effect. *IEEE Transactions on Electron Devices.* **44**, 766-774 (1997).
11. Liu, G., and Han, M., Fiber-optic gas pressure sensing with a laser-heated silicon-based Fabry-Perot interferometer. *Optics Letters.* **40**, 2461-2464 (2015).
12. Liu, G., Hou, W., Qiao, W., and Han, M., Fast-response fiber-optic anemometer with temperature self-compensation. *Optics Express.* **23**, 13562-13570 (2015).
13. Liu, G., Sheng, Q., Hou, W., and Han, M., Optical fiber vector flow sensor based on a silicon Fabry-Perot interferometer array. *Optics Letters.* **41**, 4629-4632 (2016).
14. Liu, G., Sheng, Q., Geraldo, R. L. P., Hou, W., and Han, M., A fiber-optic water flow sensor based on laser-heated silicon Fabry-Perot cavity. *Proceedings of SPIE.* **9852**, 98521B (2016).
15. Reinke, M. L., Han, M., Liu, G., Eden, G. G. v., Evenblij, R., and Haverdings, M., Development of plasma bolometers using fiber-optic temperature sensors. *Review of Scientific Instruments.* **87**, 11E708 (2016).
16. Zhang, Y., *et al.* Fringe visibility enhanced extrinsic Fabry-Perot interferometer using a graded index fiber collimator. *IEEE Photonics Journal.* **2**, 469-481 (2010).
17. Hou, W., *Ocean sensing and monitoring.* SPIE Press, (2013).
18. Hou, W., Woods, S., Jarosz, E., Goode, W., and Weidemann, A., Optical turbulence on underwater image degration in natural environments. *Applied Optics.* **51**, 2678-2686 (2012).
19. Hou, W., Jarosz, E., Woods, S., Goode, W., and Weidemann, A., Impacts of underwater turbulence on acoustical and optical signals and their linkage. *Optics Express.* **21**, 4367-4375 (2013).
20. Nootz, G., Jarosz, E., Dalgleish, F. R., and Hou, W., Quantification of optical turbulence in the ocean and its effects on beam propagation. *Applied Optics.* **55**, 8813-8820 (2016).
21. Nootz, G., Matt, S., Kanaev, A., Judd, K., and Hou, W., Experimental and numerical study of underwater beam propagation in a Rayleigh-Bénard turbulence tank. *Applied Optics.* **56**, 6065-6072 (2017).
22. Matt, S., *et al.* A controlled laboratory environment to study EO signal degradation due to underwater turbulence. *Proceedings of SPIE.* **9459**, 94590H (2015).
23. Han, M., Liu, G., and Hou, W., *Fiber-optic temperature and flow sensor system and methods.* U.S. Patent 9995628 B1 (2018).
24. Kallenbach, A., *et al.* Impurity seeding for tokamak power exhaust: from present devices *via* ITER to DEMO. *Plasma Physics and Controlled Fusion.* **55**, 124041 (2013).
25. *Alcator C-Mod.* <https://commons.wikimedia.org/wiki/File:Alcator_C-Mod_Tokamak_Interior.jpg> (2018).
26. Meister, H., Willmeroth, M., Zhang, D., Gottwald, A., Krumrey, M., and Scholze, F., Broad-band efficiency calibration of ITER bolometer prototypes using Pt absorbers on SiN membranes. *Review of Scientific Instruments.* **84**, 123501 (2013).
27. Peterson, B. J., *et al.* Development of imaging bolometers for magnetic fusion reactors. *Review of Scientific Instruments.* **79**, 10E301 (2008).
28. Liu, G., Sheng, Q., Dam, D., Hua, J., Hou, W., and Han, M., Self-gauged fiber-optic micro-heater with an operation temperature above 1000 °C. *Optics Letters.* **42**, 1412-1415 (2017).
29. Liu, G., Hou, W., and Han, M., Unambiguous peak recognition for a silicon Fabry-Perot interferometric temperature sensor. *Journal of Lightwave Technology.* **36**, 1970-1978 (2018).
30. Liu, G., Sheng, Q., Hou, W., and Han, M., High-resolution, large dynamic range fiber-optic thermometer with cascaded Fabry-Perot cavities. *Optics Letters.* **41**, 5134-5137 (2016).

Copyright © 2018 Journal of Visualized Experiments